JOURNAL OF SOLID STATE CHEMISTRY **140,** 337–344 (1998)
ARTICLE NO. SC987896

Compounds with the $YbFe_2O_4$ Structure Type: Frustrated Magnetism and Spin-Glass Behavior

R. J. Cava,*[,1] A. P. Ramirez,* Q. Huang,†[,‡] and J. J. Krajewski*

*Bell Laboratories, Lucent Technologies, Murray Hill, New Jersey, 07974; †National Institute of Standards and Technology, Gaithersburg, Maryland 20899; and ‡Materials Research Program, University of Maryland, College Park, Maryland 20742

Received February 2, 1998; in revised form May 4, 1998; accepted May 7, 1998

The $YbFe_2O_4$ structure type consists of triangular layers of lanthanide oxygen octahedra stacked with triangular double layers of transition metal oxygen triangular bipyramids. The crystallographic structures determined by neutron diffraction powder profile analysis at 300 and 11 K for new members of this structural family are reported. The compounds are found to be magnetically frustrated, by both lattice geometry and disorder. The magnetic properties of $YbCuGaO_4$, $LuCuGaO_4$, $LuZnFeO_4$, $LuCoGaO_4$, and $LuCuFeO_4$ reveal the effects of total spin, spin mixing, and interaction between spins on different sublattices on the magnetic frustration. The magnetism is increasingly frustrated as the spin on the magnetic ions is decreased.

INTRODUCTION

Magnetic materials with triangle-based lattice geometries which frustrate the long-range ordering of antiferromagnetically interacting spins at low temperatures have been the subject of considerable study in recent years. These systems display a different phenomenology from magnetic systems in which magnetic ordering is frustrated due to structural disorder (1–3). The structure types which have served as models for this geometrical frustration have been the magnetoplumbites (4–6), delafossites (7–9), pyrochlores (10, 11), and jarosites (12–17). Here we report the structural and magnetic characterization of a new family of magnetically frustrated materials with the $YbFe_2O_4$ structure type (18), which is based on the stacking of triangular rare earth and transition metal layers. The materials described here are of the type $Ln^{3+}M^{2+}M'^{3+}O_4$, where Ln is either Lu or Yb and M and M' are late 3d transition metals. The small rare earths are in octahedral coordination with oxygen and form a triangular layer. The transition metals are in triangular double layers in which the $M(M')$–O in-plane bonding geometry has approximately 120° O–$M(M')$–O bond angles. The transition metals are disordered in the triangular double layer. These materials are unusual in that they are both geometrically and site-disorder frustrated and that they have two magnetic sublattices, both of which have triangular geometries. The chemistry of the system is widely variable, allowing atoms of different spins to be included on the different sublattices, an aspect which has not been widely explored in other frustrated magnetic systems. The crystal structures of representative members of the family were determined by neutron diffraction powder profile analysis at ambient temperature and 11 K in order to provide a basis for discussion of the magnetic properties.

[1] Present address: Department of Chemistry and Materials Institute, Princeton University, Princeton NJ 08540.

EXPERIMENTAL

Synthesis

The compounds chosen for study are a derivative of those first described by Kimuzuka and Takayama (20, 21) in phase equilibria studies of Yb_2O_3–MO–M'_2O_3 chemical systems. For the purpose of the magnetic studies, we concentrated primarily on the synthesis and characterization of previously unreported materials with Lu on the rare earth site, due to its filled 4f orbitals and resultant nonmagnetic character. The compounds $LuCuGaO_4$, $LuCuFeO_4$, $LuZnFeO_4$, $LuCoGaO_4$, and $YbCuGaO_4$ were synthesized from stoichiometric mixtures of Yb_2O_3, Lu_2O_3, Fe_2O_3, CuO, Ga_2O_3, ZnO, and Co_3O_4. Long heating times, between 125 and 175 h, with multiple intermediate grindings were required in all cases to obtain single phase polycrystalline materials. For $YbCuGaO_4$, $LuCuGaO_4$, and $LuCuFeO_4$ the final treatment was 1125°C in O_2. For $LuZnFeO_4$ and $LuCoGaO_4$ the final treatments were in air at 1300°C. All samples were determined to be phase pure by powder X-ray diffraction before further study.

Structure Determination

The powder neutron diffraction measurements were performed at the reactor of the National Institute of Standards

0022-4596/98 $25.00

and Technology Center for Neutron Research. The diffraction intensity data were collected using the BT-1 high resolution powder diffractometer with neutron beams of wavelength 1.5396(1) Å produced by a Cu 311 monochromator. Collimators with horizontal divergence of 15′, 20′, and 7′ full-width at half-maximum were used before and after the monochromator and after the sample, respectively. The intensities were measured in steps of 0.05° in the 2θ range 3–168°. The structure refinements were carried out using the program GSAS. The neutron scattering lengths used in the calculations were 0.73, 1.24, 0.253, 0.772, 0.945, 0.568, 0.729, and 0.581 ($\times 10^{-12}$ cm) for Lu, Yb, Co, Cu, Fe, Zn, Ga, and O, respectively.

The results of the crystal structure refinements are summarized in Tables 1 and 2. The crystallographic cell found in the neutron diffraction measurements for all compounds is of the same general type as found by X-ray diffraction for $YbFe_2O_4$, space group $R\bar{3}m$ with $a \approx 3.4$ and $c \approx 24$. Unlike the published model for $YbFe_2O_4$, however, it was found that the lanthanide ions are displaced from their ideal positions. The refinements for different structural models for $LuCuGaO_4$ are presented in Table 1 to illustrate this finding. The first column (model I) shows the results of structural refinements in which the Lu is in the ideal 3*a* (0,0,0) position. It can be seen that the agreement index (*R*) values are relatively large and that the isotropic thermal parameter for the Lu atom is also anomalously large. The second column (model II) shows the refinement in which Lu atom is allowed to display anisotropic thermal vibration. The agreement factors are dramatically improved. The thermal parameter for Lu is very large along the *c* axis. This large thermal parameter is an indication of static disorder of the Lu atom positions along *c*. Column III presents the final structural model (model III), in which the displacement of the Lu atoms from their ideal position is described by placing the Lu in the 6*c* (0,0,*z*) positions. The *z* parameter is defined to high precision, the thermal parameters are now of normal magnitudes, and the agreement indices are very good, indicating the correctness of this model. The pairs of related sites (0,0,*z*) and (0,0,*z*) with $z \approx 0.008$, are occupied with 50% statistical occupancy. The amount of displacement from the ideal position is temperature independent and different for the different compounds, and in some cases is relatively small, as shown in Table 2. The metal atoms M^{2+} and M^{3+} are completely disordered in 6*c* (0,0,*z*) positions with $z \approx 0.21$.

TABLE 1
Refinements in Different Models for $LuCuGaO_4$ at 296 K [Space Group $R\bar{3}m$ (No. 166); Positions for Sites 3*a* and 6*c* Are (0,0,0) and (0,0,*z*), Respectively]

Atom	Site	Parameter	Model I	Model II	Model III
		a (Å)	3.44060(7)	3.44070(5)	3.44071(5)
		c (Å)	24.2907(6)	24.2917(4)	24.2918(4)
		V (Å)	249.02(1)	249.05(1)	249.04(1)
Lu	3*a*	*B* (Å^2)	1.79(3)		
		$B_{11}=B_{22}$ (Å^2)		0.45(3)	
		B_{33} (Å^2)		5.5(1)	
		B_{12} (Å^2)		0.23(2)	
	6*c*	*z*			0.00904(7)
		B (Å^2)			0.52(4)
		n			0.5
Ga/Cu	6*c*	*z*	0.21391(5)	0.21395(4)	0.21404(4)
		B (Å^2)	0.79(2)		0.86(2)
		$B_{11}=B_{22}$ (Å^2)		0.85(2)	
		B_{33} (Å^2)		0.82(4)	
		B_{12} (Å^2)		0.43(1)	
O(1)	6*c*	*z*	0.29183(7)	0.29142(5)	0.29135(5)
		B (Å^2)	1.35(3)		1.18(2)
		$B_{11}=B_{22}$ (Å^2)		1.30(3)	
		B_{33} (Å^2)		0.96(5)	
		B_{12} (Å^2)		0.65(2)	
O(2)	6*c*	*z*	0.12918(9)	0.12907(6)	0.12898(6)
		B (Å^2)	2.53(4)		2.42(3)
		$B_{11}=B_{22}$ (Å^2)		2.23(8)	
		B_{33} (Å^2)		3.03(8)	
		B_{12} (Å^2)		1.12(2)	
		R_p (%)	7.20	5.29	5.34
		R_{wp} (%)	9.32	6.63	6.69
		χ^2	2.786	1.41	1.436

A detailed report of the refined crystallographic parameters for all compounds at 296 and 11 K is presented in Table 2. An example of the agreement between the observed and calculated neutron powder diffraction profiles is presented in Fig. 1 and $LuCuFeO_4$ at 11 K. There was no indication of long-range magnetic order in the neutron diffraction experiments at 296 or 11 K for any of the compounds. For $LuCuFeO_4$ however, extra scattered neutron intensity was found in a broad peak at $\approx 18°$ 2θ at 11 K, shown as an inset in Fig. 1, characteristic of short-range spin-glass type ordering of the magnetic moments at low temperatures. This is consistent with the magnetic susceptibility results for this compound, as described below. The diffuse peak was also observed, although considerably weaker in intensity, in $LuZnFeO_4$ and $LuCoGaO_4$ at 11 K.

The crystal structure for the compounds is shown in Fig. 2, using the atomic coordinates of $LuCuFeO_4$ as an example. The structure consists of double layers of MO_5 triangular bipyramids interleaved with triangular layers of LnO_6 octahedra. The lanthanide positions, in triangular layers perpendicular to *c*, are shown as pairs of black dots in the figure. (Only one of each pair is occupied.) The Lu and Yb are in distorted octahedral coordination with oxygen (see Table 3), shown in more detail in Fig. 3. Of central importance to the interpretation of the magnetic properties is the fact that the transition metal ions for all compounds are not ordered in different crystallographic sites but are rather statistically disordered in the 6*c* (0,0,*z*) positions with

TABLE 2
Structural Parameters of $LnM^{2+}M^{3+}O_4$ (Ln = Lu, Yb; M^{2+} = Cu, Co, Zn; M^{3+} = Ga. Fe) at 296 K (First Line) and 11 K (Second Line) [Space Group $R\bar{3}m$ (No. 166); Position for Site 6c is (0,0,z); $M = 0.5M^{2+} + 0.5M^{3+}$]

Atom	Site	Parameter	$LuCuGaO_4$	$LuCoGaO_4$	$YbCuGaO_4$	$LuCuFeO_4$	$LuZnFeO_4$
		a (Å)	3.44071(5)	3.4062(1)	3.45910(6)	3.46618(5)	3.4080(1)
			3.43437(6)	3.4024(2)	3.45195(5)	3.46328(5)	3.4029(1)
		c (Å)	24.2918(4)	25.220(1)	24.1992(5)	24.1382(4)	25.369(1)
			24.2958(5)	25.207(1)	24.1711(5)	24.1331(4)	25.361(1)
		V (Å^3)	249.05(1)	253.41(3)	250.76(1)	251.152(9)	255.17(2)
			248.23(1)	252.71(3)	249.43(1)	250.68(1)	254.34(2)
Ln	6c	z	0.00940(7)	0.0071(2)	0.00864(5)	0.00941(7)	0.0077(1)
			0.00926(7)	0.0064(2)	0.00863(5)	0.00955(7)	0.0077(1)
		B (Å^2)	0.52(4)	0.32(6)	0.48(2)	0.51(2)	0.95(5)
			0.28(3)	0.46(6)	0.25(2)	0.34(2)	0.52(5)
		n	0.5	0.5	0.5	0.5	0.5
			0.5	0.5	0.5	0.5	0.5
M	6c	z	0.21404(4)	0.2153(1)	0.21381(4)	0.21390(3)	0.21557(5)
			0.21422(4)	0.2150(1)	0.21381(4)	0.21389(3)	0.21570(5)
		B (Å^2)	0.86(2)	0.52(4)	0.79(2)	0.71(2)	0.38(2)
			0.57(2)	0.52(4)	0.52(2)	0.53(2)	0.10(2)
O(1)	6c	z	0.29135(5)	0.2917(1)	0.29150(6)	0.29180(5)	0.29229(7)
			0.29134(5)	0.2915(1)	0.29154(6)	0.29180(5)	0.29200(7)
		B (Å^2)	1.18(2)	0.90(4)	1.05(3)	1.02(2)	1.59(3)
			1.05(2)	0.84(4)	0.80(2)	1.00(3)	1.35(4)
O(2)	6c	z	0.12898(6)	0.1286(1)	0.12893(7)	0.12804(5)	0.12772(7)
			0.12904(6)	0.1286(1)	0.12897(7)	0.12803(6)	0.12741(7)
		B (Å^2)	2.42(3)	1.64(3)	2.26(4)	1.82(3)	1.84(3)
			2.16(3)	1.55(3)	2.11(3)	1.75(4)	1.60(3)
R_p (%)			5.34	5.59	4.52	4.99	5.42
			6.08	6.58	4.85	5.57	5.90
R_{wp} (%)			6.69	7.40	5.64	6.16	6.62
			7.71	8.69	5.92	6.89	7.25
χ^2			1.436	1.686	1.547	1.563	1.592
			1.397	1.540	1.907	1.930	1.953

$z \approx 0.21$. The geometry of these positions is shown in Fig. 2, which emphasizes the transition metal–oxygen bonding in the triangular double layer. The individual triangular metal layers in the double layer are arranged such that each metal has three nearest neighbor metals in the adjacent layer and is therefore also frustrated with respect to that layer. The O–M–O bond angles in the triangular plane (Table 3) are slightly distorted from the ideal (from 120 to 118°) due to the fact that the metal and oxygen atoms are not exactly coplanar. The metal–oxygen bond lengths to the apical oxygens at the periphery of the double layers (O(1)) are shorter in all cases than to the oxygens within the metal planes or the apical oxygens in the adjacent M–O plane (O(2)). Selected interatomic distances and bond angles for all compounds are summarized in Table 3.

In the LnO_6 layers, the Ln ion is in a distorted octahedron, coordinated to three oxygen above and three oxygen below (Fig. 3). The oxygen atoms bond to one M atom each in the adjacent layers, i.e., to a total of three M atoms above the Ln plane and three M atoms below. The displacement of an Ln atom from the ideal (0,0,0) position can be attributed to the local distribution of M atoms in the neighboring layers. The configuration shown in Fig. 3 is the particular case in which the M distribution results in three M^{2+} atoms in the upper layer and three M^{3+} atoms in the lower layer, resulting in a shift of the Ln ion toward the lower layer, and represents one extreme condition for the local displacement. More uniform distribution of M^{2+} and M^{3+} in the neighboring layers will result in the intervening Ln being closer to the ideal position: the Ln position found in the refinement is therefore considered to be an average of the possible positions in a distribution of local near neighbor M configurations.

Magnetic Properties

The magnetization (M) was measured using a commercial SQUID magnetometer. Where the magnetic susceptibility

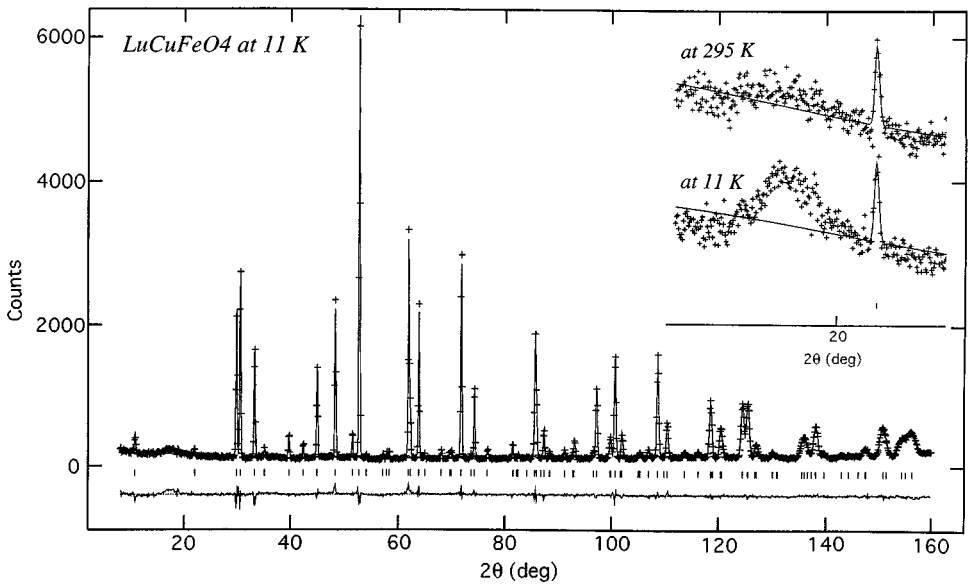

FIG. 1. Plot of observed (crosses) and calculated (solid line) intensity profiles for $LuCuFeO_4$ at 11 K. The lower part of the figure shows the difference plot, $I(\text{obs}) - I(\text{calc})$. The inset shows a broad peak at $\approx 18^\circ$ 2θ observed only at 11 K.

(χ) is shown, the magnetization has been divided by the applied field, which was either 0.1 or 0.5 tesla. The specific heat (C) was measured using a semiadiabatic heat pulse technique involving a sapphire calorimeter and resistive heating and temperature-sensing elements. Since the samples were in ceramic powder form, to facilitate thermal equilibration among the grains, we pressed the sample with silver powder into a hard disk. The contribution to the specific heat from the silver, as well as the calorimeter, was measured independently.

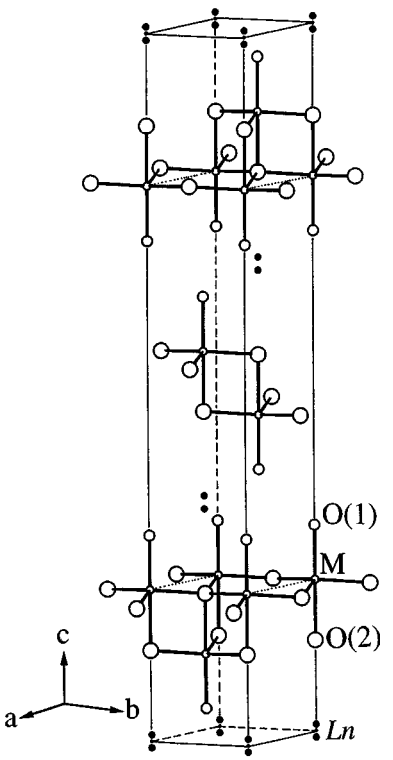

FIG. 2. The crystal structure of $LuCuFeO_4$, a representative of the $LnM^{2+}M'^{3+}O_4$ family. The lanthanide atoms (black dots) are found in two different positions with 50% occupancy each, separated by a small distance along the c axis, as shown. "M" refers to the position occupied by the mixture of M'^{3+} and M^{2+} atoms.

The temperature dependent magnetic susceptibilities of the compounds are summarized in Figs. 4–8. The data for LuZnFeO$_4$ are presented in Fig. 4 for temperatures between

TABLE 3

Selected Interatomic Distances (Å) and Angles (deg) for $LnM^{2+}M^{3+}O_4$ (Ln = Lu, Yb; M^{2+} = Cu, Co, Zn; M^{3+} = Ga, Fe) at 296 K (First Line) and 11 K (Second Line) [$M = 0.5M^{2+} + 0.5M^{3+}$]

		$LuCuGaO_4$	$LuCoGaO_4$	$YbCuGaO_4$	$LuCuFeO_4$	$LuZnFeO_4$
Ln–O(1)	×3	2.341(1)	2.318(3)	2.3410(9)	2.349(1)	2.323(2)
	×3	2.342(1)	2.310(3)	2.3362(9)	2.349(1)	2.325(2)
Ln–O(1)	×3	2.1417(7)	2.151(2)	2.1525(7)	2.1462(7)	2.142(1)
	×3	2.1366(7)	2.159(2)	2.1482(7)	2.1433(7)	2.142(1)
M–O(1)		1.878(2)	1.927(4)	1.880(2)	1.880(2)	1.946(2)
		1.874(2)	1.927(5)	1.879(7)	1.880(2)	1.935(2)
M–O(2)		2.066(2)	2.188(4)	2.054(2)	2.073(2)	2.229(2)
		2.070(2)	2.177(4)	2.051(2)	2.072(2)	2.239(2)
M–O(2)	×3	2.0004(2)	1.9846(5)	2.0101(2)	2.0120(2)	1.9837(3)
	×3	1.9977(2)	1.9815(6)	2.0060(2)	2.0102(2)	1.9803(3)
O(1)–M–O(2)	×3	96.75(5)	97.7(1)	96.50(6)	95.93(4)	97.31(6)
	×3	96.93(5)	97.6(1)	96.54(6)	95.91(5)	97.20(6)
O(2)–M–O(2)	×3	83.25(5)	82.3(1)	83.50(6)	84.07(4)	82.69(6)
	×3	83.07(5)	82.4(1)	83.46(6)	84.09(5)	82.80(6)
O(2)–M–O(2)	×3	118.64(2)	118.22(5)	118.74(2)	118.95(2)	118.41(3)
	×3	118.56(2)	118.30(5)	118.72(2)	118.95(2)	118.46(3)

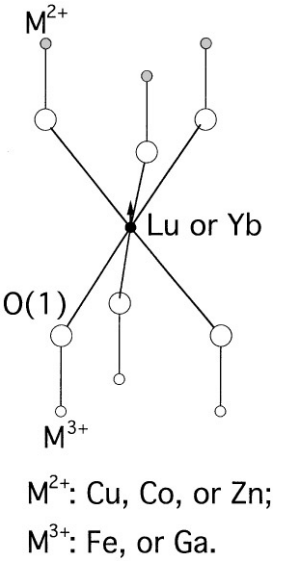

FIG. 3. Proposed model for the split lanthanide position, to accommodate short-range order among the M^{2+} and M'^{3+} atoms.

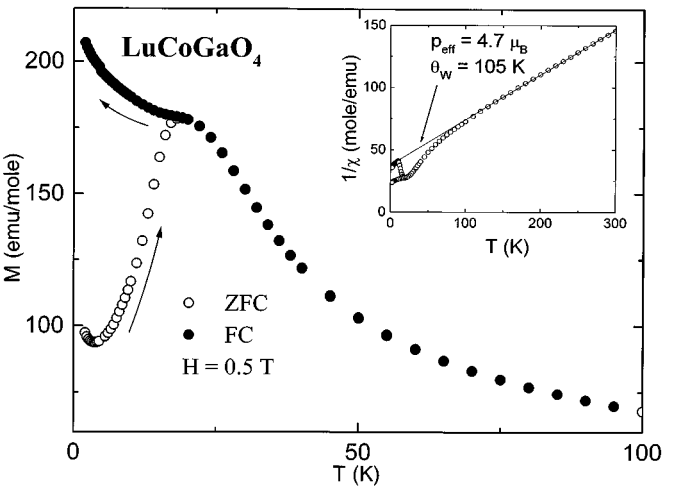

FIG. 5. Temperature dependence of the field cooled and zero field cooled magnetic susceptibility for $LuCoGaO_4$. Inset, inverse χ vs T.

100 and 4 K. The inset shows the plot of reciprocal susceptibility $1/\chi$ vs T for the same material. The fit to the high temperature data indicate an antiferromagnetic interaction among the spins, with a Weiss temperature (θ_W) of 670 K and a moment of approximately 5.8 μ_B per formula unit. The iron valence in this compound is restricted by the other atoms present, which are not transition metals, to be 3+. With expected moments of 5.9 and 1.7 μ_B for Fe^{3+} in the high spin and low spin configurations respectively, the measured moment of 5.8 μ_B indicates that the Fe is in the high spin state. The field cooled and zero field cooled data are presented in the figure. They show a difference starting at about 25 K, charcteristic of a spin-glass transition at the temperature (T_g). The large θ_W/T_g ratio indicates significant frustration of the moments, i.e. ordering does not occur in the expected temperature range of approximately θ_W to $\theta_W/2$. In addition, the decrease in the susceptibility in the spin-glass transition is relatively small, suggesting that many of the spins may not be participating in the apparent spin freezing. The specific heat study described below, does suggest, however, that this feature represents the freezing of the majority of the Fe spins. The broad, weak magnetic peak observed at low temperature in the neutron scattering measurements is consistent with the lack of a sharp feature in the susceptibility. There is a subtle feature in the susceptibility immediately above the spin-glass temperature, visible

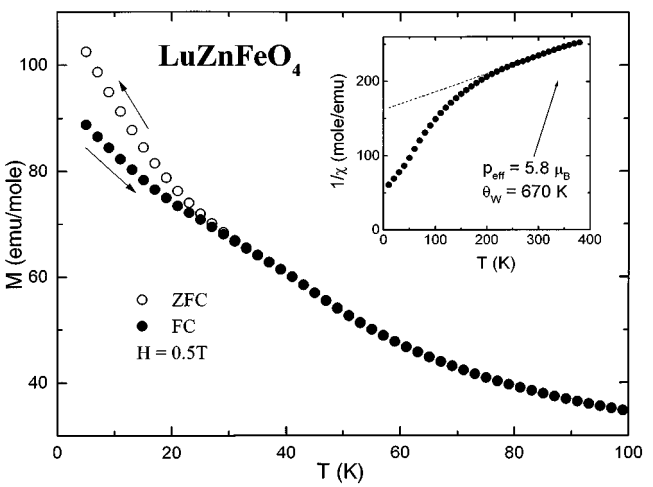

FIG. 4. Temperature dependence of the field cooled and zero field cooled magnetic susceptibility of $LuZnFeO_4$. Inset, inverse χ vs T.

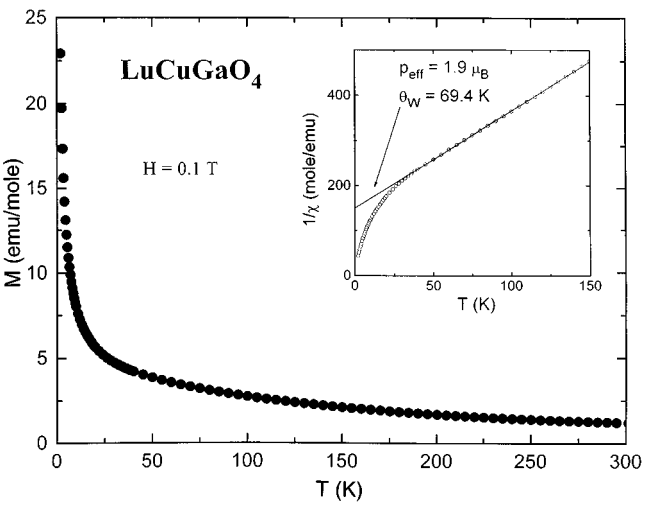

FIG. 6. Temperature dependence of the linear and inverse field cooled susceptibility for $LuCuGaO_4$ from 300 to 4 K. Inset, inverse χ vs T.

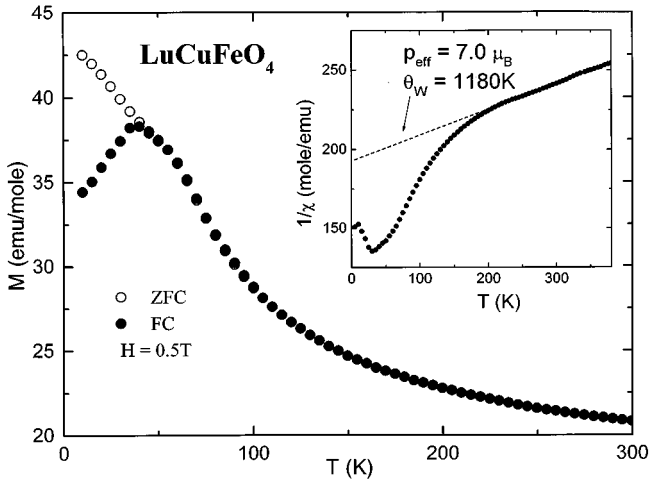

FIG. 7. Temperature dependence of linear and inverse (inset) χ vs T for one material with two magnetic ions mixed on the triangular double layers, $LuCuFeO_4$.

in both linear (as a broad bump near 40 K) and inverse χ plots. This is possibly due to the occurrence of short-range order precceding the spin freezing.

For $LuCOGaO_4$, Fig. 5, the susceptibility resembles that of a more classical spin glass transition, with a significant deviation between the field cooled and zero field cooled susceptibilities at a T_g of about 20 K and a significant loss of susceptibility below the ordering transition. Again, the valence of the transition metal is fixed by the other ions present, this time to $2+$. The high temperature susceptibility (inset, Fig. 5), yields an effective moment of 4.7 μ_B per formula unit, consistent with that expected for Co^{2+} in its high spin state. For this meterial the interactions are again antiferromagnetic in nature, this time with a θ_W of 105 K. The $1/\chi$ vs T plot indicates the onset of long range correlations in the susceptibility near 100 K as a deviation of the susceptibility from the straight line behavior observed at higher temperatures.

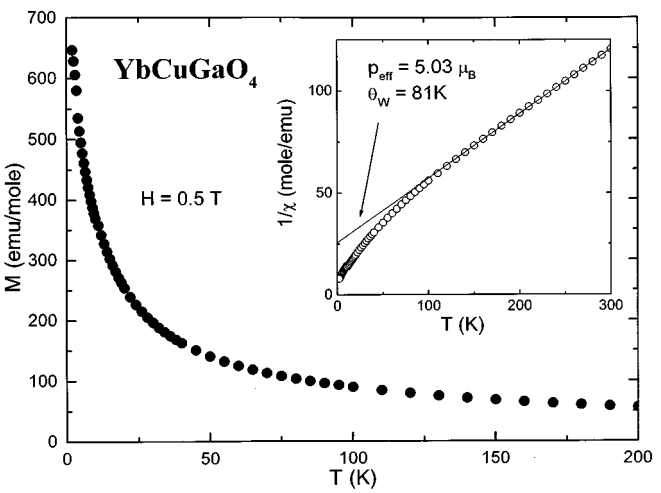

FIG. 8. Temperature dependent linear and inverse (inset) magnetic susceptibility for $YbCuGaO_4$, a material with magnetic atoms on the triangular lanthanide and double layer transition metal sites.

The most interesting case for the materials in which only one magnetic ion is present is for $LuCuGaO_4$, for which the copper valence is $2+$. The data are shown in Fig. 6 as both linear χ and inverse χ plots. No magnetic ordering is observed to 4 K. The inset to the figure shows that the high temperature susceptibility is well described by the Curie–Weiss law, with a moment of 1.9 μ_B per formula unit, consistent with what is expected for Cu^{2+}, and a θ_W characteristic of antiferromagnetic interactions of 69 K. The inset shows the onset of correlations at approximately 40 K, but there is no evidence of magnetic ordering. The copper analog therefore shows more magnetic trustration than either the Co or Fe compounds.

Mixtures of magnetic ions are also possible in this structure type, both on the double layer transition metal sublattice, and by having magnetic ions on both rare earth and transition metal sublattices. We were unable to prepare compounds with only magnetic ions on the lanthanide sublattice, such as $YbZnGaO_4$, in sufficient purity to study their properties. The magnetic properties of $LuCuFeO_4$, in which two magnetic ions are mixed on the transition metal sites are presented in Fig. 7. By analogy to the compounds just described, it can be expected that this compound contains a mixture of Cu^{2+} and Fe^{3+}. The inset of Fig. 7 shows that there has been a dramatic increase in the strength of the antiferromagnetic interaction, now with a Weiss temperature θ_W of 1180 K, a factor of 2–17 increased over the interaction strengths in the single magnetic ion Fe or Cu cases, due to the greatly increased occupancy of magnetic atoms on the triangular double layers. The main panel shows that the field cooled and zero field cooled susceptibilities deviate from each other at 40 K. Again, the large value of θ_W/T_g is indicative of the strong frustration of the spins; however, the increase in T_g does not scale linearly with the increase in interaction strength. The high temperature data indicate an effective magnetic moment of approximately 7.0 μ_B per formula unit, in agreement with what is expected for a mixture of Cu^{2+} and Fe^{3+} high spin.

The temperature dependent magnetic susceptibility for $YbCuGaO_4$ is presented in Fig. 8. In this case, there are magnetic and nonmagnetic ions mixed in the triangular transition metal double layer, and the lanthanide layer is fully occupied by the magnetic Yb^{3+} (one unpaired electron in the 4f obrital). As in the case of $LuCuGaO_4$, no magnetic ordering is observed above 4 K. The inset of Fig. 8 reveals interesting differences between this case of magnetic mixing and the case where the transition metal double layer is fully occupied by magnetic atoms. The inset shows that the interactions are still antiferromagnetic, but that the

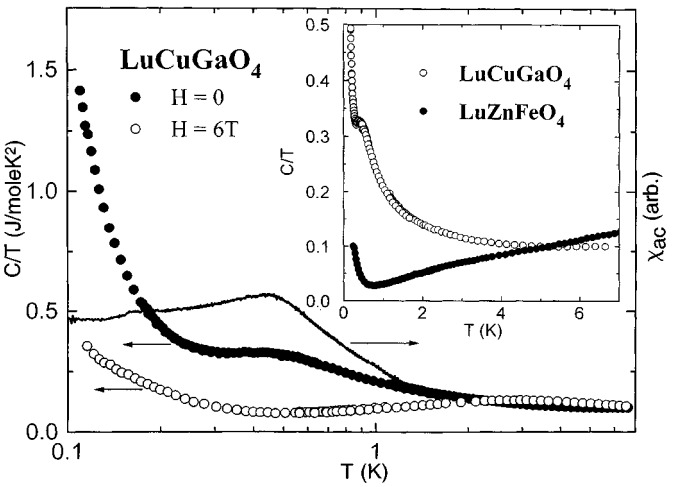

FIG. 9. Specific heat at low temperatures for $LuCuGaO_4$ at 0 and 6 tesla applied magnetic field, and the low field AC susceptibility, showing the spin-glass transition (main panel). Inset: Comparison of the specific heats at low temperature in zero applied for $LuCuGaO_4$ and $LuZnFeO_4$.

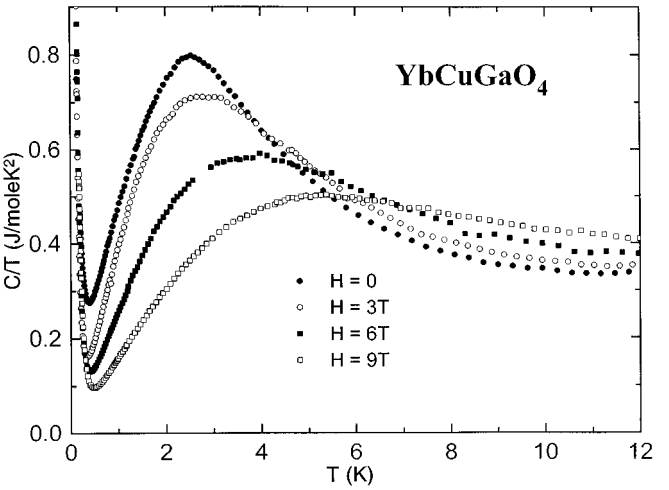

FIG. 10. Specific heat at low temperatures for $YbCuGaO_4$ in different applied magnetic fields.

interaction strength is only slightly increased (from 69 to 81 K). This suggests that the two magnetic sublattices are only weakly coupled. The high temperature susceptibility indicates that the effective moment is, in this case, large, 5 μ_B per formula. For a magnetic moment of 1.73 μ_B per copper, this indicates an effective moment of 4.7 μ_B per Yb^{3+}, close to the ideal value 4.5 μ_B, indicating that the magnetic moments are as expected. The data show that the lanthanide lattice is likely frustrated in itself, as there is no ordering above 4 K. Deviations from Curie–Weiss behavior can be seen at 100 K, consistent with the θ_W of 81 K.

The magnetic and thermodynamic properties of the phases which did not reveal their magnetic ground state above 4 K were studied at lower temperatures. For the specific heat data presented in Figs. 9 and 10, the lattice contribution to the specific heat is approximately 10% of the total at 12 K and does not affect the discussion of the magnetic specific heat. The magnetic susceptibility and specific heat for $LuCuGaO_4$ are presented in Fig. 9 (main panel) for temperatures between 6 K and 150 mK. The magnetic susceptibility (AC, 100 Hz) shows the presence of a broad peak at approximately 0.45 K, which we attribute to the spin-glass ordering temperature. Coupled with the Cuire temperature of 69 K, this system is seen to be highly frustrated. The figure also shows the specific heat measured in zero applied and in a field of 6 tesla. The data at zero field show the presence of an increase in C/T at very low temperatures and an additional broad feature at 0.45 K corresponding to the peak in the susceptibility. This 0.45 K feature is seen to be suppressed by the magnetic field. The bulk of the entropy is shifted into a broad peak centered at about 3 K at a field of 6 tesla. The behavior of the peak position with field implies that the peak derives from weakly interacting spins. The shape of the peak is far broader than what is expected from a Schottky anomaly, especially on the low temperature side, and this is the main effect of the interactions evidenced also in the susceptibility.

The inset to Fig. 9 compares the specific heat at low temperatures for both $LuCuGaO_4$ and $LuZnFeO_4$. It can be seen in this comparison that the entropy for the latter compound has already been frozen out by 6 K, indicating that the rather weak feature observed in the susceptibility (Fig. 4) really does represent the spin-glass ordering of the Fe moments. The upturn seen in C/T at the lowest temperature might have two possible causes. In $LuZnFeO_4$, it is likely the result of nuclear hyperfine levels, perhaps those of the Lu^{175} isotope. In the cases of $LuCuGaO_4$ and $YbCuGaO_4$ (data shown in Fig. 10), the upturn seems too large to be due solely to the nuclear levels. The low temperature specific heat for $YbCuGaO_4$ show a clearly defined broad peak in the specific heat is observed at approximately 2.4 K, which we attribute to a spin-glass transition on the Yb sublattice. The transition for this material has been measured at several magnetic field up to 9 T. The data show the expected transformation from a short-range ordered peak to a Schottky anomaly, typical of the behavior seen in correlated systems with an interaction energy lower than the Zeeman energy. The integrated entropy for the data shown do not appreciably exceed R ln 2, that expected for the Yb moment. It seems possible, therefore, that the upturn is the result of the high temperature tail of the transition, either spin-glass or conventional long-range order, among the Cu spins at temperatures lower than those accessed in these experiments. The magnetic characterization of all materials studied is summarized in Table 4.

TABLE 4
Magnetic Characterization of $YbFe_2O_4$ Type Compounds p_{eff}, Effective Magnetic Moment; θ_W, Weiss Temperature; T_g, Spin-Glass Temperature

Compound	p_{eff}	θ_W (*K*)	T_g (K)	θ_W/T_g
$LuZnFeO_4$	5.8	670	25	27
$LuCoGaO_4$	4.7	105	19	6
$LuCuGaO_4$	1.9	69	0.45	153
$LuCuFeO_4$	7.0	1180	40	30
$YbCuGaO_4$	5.0	81	2.5	32

SUMMARY AND CONCLUSION

The crystal structures and magnetic properties of a series of previously uncharacterized compounds with the $YbFe_2O_4$ structure type have been described. The compounds are unusual in that they are made from stacking two triangular geometry planar sublattices into which different concentrations and types of magnetic atoms can be introduced. Magnetic frustration is observed as a general characteristic of the structure type, with the copper containing compound $LuCuGaO_4$ of particular interest due to the relatively high degree of frustration. All compounds studied here are electrically insulating. The broad chemical stability of this structure type suggests that it might be possible to investigate the effect of the introduction of charge carriers, through full or partial chemical substitution, on the magnetic properties of the frustrated magnetic lattice in this case, something which has not been widely pursued for other frustrated magnetic materials.

REFERENCES

1. A. P. Ramirez, *Annu. Rev. Mat. Sci.* **24,** 453 (1994).
2. S.-H. Lee, C. Broholm, G. Aeppli, A. P. Ramirez, T. G. Perring, C. J. Carlile, M. Adams, T. J. L. Jones, and B. Hessen, *Europhys. Lett.* **35,** 127 (1996).
3. J. L. Tholence, *Physica B*, **126,** 157 (1984).
4. X. Obradors, A. Labarta, A. Isalgue, J. Tejada, J. Rodriguez, and M. Pernet, *Solid State Commun.* **65,** 189 (1988).
5. A. P. Ramirez, G. P. Espinosa, and A. S. Cooper, *Phys. Rev. Lett.* **64,** 2070 (1992).
6. S.-H. Lee, C. Broholm, G. Aeppli, T. G. Perring, B. Hessen, and A. Taylor, *Phys. Rev. Lett.* **76,** 4424 (1996).
7. K. Hirakawa, H. Kadowaki, and K. Ubukoshi, *J. Phys. Soc. Jpn.* **54,** 3526 (1985).
8. A. P. Ramirez, R. Jager-Waldau, and T. Siegrist, *Phys. Rev. B* **43,** 10461 (1991).
9. A. Tauber, W. M. Moller, and E. Banks, *J. Solid State Chem.* **4,** 138 (1972).
10. J. E. Greedan, M. Sato, X. Yan, and F. S. Razavi, *Solid State Commun.* **59,** 895 (1986).
11. M. J. P. Gingras, C. V. Stager, N. P. Raju, B. D. Gaulin, and J. E. Greedan, *Phys. Rev. Lett.* **78,** 947 (1997).
12. M. Takano, T. Shinjo, and T. Tanaka, *J. Phys. Soc Jpn.* **30,** 1049 (1971).
13. M. G. Townsend, G. Longworth, and E. Roudaut, *Phys. Rev. B* **33,** 4919 (1986).
14. A. Keren, K. Kojima, L. P. Le, G. M. Luke, W. D. Wu, Y. J. Uemura, M. Takano, H. Dabkowska, and M. J. P. Gringras, *Phys. Rev*, *B* **53,** 6451 (1996).
15. S.-H. Lee, C. Broholm, M. F. Collins, L. Heller, A. P. Ramirez, C. Kloc, E. Bucher, R. W. Erwin, and N. Lacevic, *Phys Rev. B* **56,** 8091 (1997).
16. A. S. Wills and A. Harrison, *J. Chem. Soc*., *Faraday Trans.* **92,** 2162 (1996).
17. S. A. Earle, A. P. Ramirez, and R. J. Cava, *Physica B*., in press.
18. K. Kato, I. Kawada, N. Kimuzuka, and T. Katsura, *Z. Kristallogr.* **141,** 314 (1975).
19. N. Kimizuka and E. Takayama, *J. Solid. State Chem.* **40,** 109 (1981).
20. N. Kimizuka and E. Takayama, *J. Solid State Chem.* **43,** 278 (1982).